Article

Not peer-reviewed version

Advancing BiVO4 Photoanode Activity for Ethylene Glycol Oxidation via Strategic pH Control

Jun-Yuan Cui , Tian-Tian Li , Long Chen , Jian-Jun Wang *

Posted Date: 17 May 2024

doi: 10.20944/preprints202405.1127.v1

Keywords: BiVO4 photoanode; ethylene glycol oxidation; pH control; photoelectrochemical

Article

Advancing $BiVO_4$ Photoanode Activity for Ethylene Glycol Oxidation via Strategic pH Control

Jun-Yuan Cui [1], Tian-Tian Li [1], Long Chen [1] and Jian-Jun Wang [1,2,*]

[1] State Key Laboratory of Crystal Materials, Shandong University, Jinan, 250100, PR China; 202132830@mail.sdu.edu.cn (J.Y.-C.); litiantian@mail.sdu.edu.cn (T.-T.L.); 202232804@mail.sdu.edu.cn (L.C.)
[2] Shenzhen Research Institute, Shandong University, Shenzhen, 518057, PR China
* Correspondence: wangjianjun@sdu.edu.cn

Abstract: The photoelectrochemical (PEC) conversion of organic small molecules offers a dual benefit of synthesizing value-added chemicals and concurrently producing hydrogen (H_2). Ethylene glycol, with its dual hydroxyl groups, stands out as a versatile organic substrate capable of yielding various C1 and C2 chemicals. In this study, we demonstrate that pH modulation markedly enhances the photocurrent of $BiVO_4$ photoanodes, thus facilitating the efficient oxidation of ethylene glycol while simultaneously generating H_2. Our findings reveal that in a pH=1 ethylene glycol solution, the photocurrent density at 1.23 V vs. RHE can attain an impressive 7.1 mA cm^{-2}, significantly surpassing the outputs in neutral and highly alkaline environments. The increase in photocurrent is attributed to the augmented adsorption of ethylene glycol on $BiVO_4$ under acidic conditions, which in turn elevates the activity of the oxidation reaction, culminating in the maximal production of formic acid. This investigation sheds light on the pivotal role of electrolyte pH in the PEC oxidation process and underscores the potential of the PEC strategy for biomass valorization into value-added products alongside H_2 fuel generation.

Keywords: $BiVO_4$ photoanode; ethylene glycol oxidation; pH control; photoelectrochemical

---

1. Introduction

The surge in global energy demand and growing environmental concerns are propelling the advancement of green energy and renewable chemicals[1–3]. Molecular hydrogen serves as both a fundamental building block for the chemical industry and a promising carbon-free energy carrier[4,5]. Over the past few decades, photoelectrochemical (PEC) water splitting has emerged as a viable method to harness solar energy and generate clean hydrogen fuel[6–8]. However, the sluggishness of the oxygen evolution reaction (OER) at the anode has been a major hurdle in PEC water splitting, leading to high energy consumption[9–11].

To address this challenge, it is proposed to replace the OER with the oxidation of small molecules with lower oxidation potentials[12]. This strategy promises higher energy efficiencies and greater current density. Polyethylene terephthalate (PET), a widely used plastic, is a prime candidate for degradation and recycling due to its versatile properties[13,14]. Ethylene glycol, a hydrolysis byproduct of PET, is particularly notable for its annual production volume and favorable properties, including low toxicity and high energy density[15–17]. The selective oxidation of biomasses such as ethylene glycol could lead to the production of valuable compounds like glycolic acid, formic acid, and oxalic acid[17,18]. Integrating biomass oxidation with hydrogen evolution reactions could enhance current output at lower potentials, potentially reducing issues like photocorrosion[19,20]. Repurposing discarded materials like ethylene glycol without relying on fossil fuels can significantly contribute to sustainability efforts. Thus, the rational usage of ethylene glycol is highly desirable but still challenging.

Among the various photoanodes, $BiVO_4$ stands out for its cost-effectiveness, narrow bandgap enabling suitable light absorption, and high activity[21–23]. It has found widespread application in

Preprints.org (www.preprints.org) | NOT PEER-REVIEWED | Posted: 17 May 2024 doi:10.20944/preprints202405.1127.v1

the PEC oxidation of biomass, coupled with hydrogen production. While $BiVO_4$ has been extensively studied for PEC glycerol oxidation[24–27], studies on other alcohols are limited. For example, Liu et al. explored the impact of pH on PEC glycerol oxidation, finding that glycerol adheres better to $BiVO_4$ at lower pH levels, facilitating charge transfer and catalyzing the conversion of glycerol into derivatives under photoelectrochemical conditions[27]. The pH of the electrolyte has emerged as a crucial factor influencing the PEC performance in glycerol oxidation[28], with acidic electrolytes promoting the oxidation process. To broaden the scope of its applications to other alcohols, understanding the effect of electrolyte pH on PEC ethylene glycol oxidation on $BiVO_4$ is essential yet unexplored. Here, we systematically investigate the influence of electrolyte pH on the PEC performance for ethylene glycol oxidation and elucidate its underlying mechanism.

2. Results and Discussion

2.1. Synthesis and structural characterizations of the $BiVO_4$ photoanode

The nanoporous $BiVO_4$ films were synthesized with minor adjustments to a previously established protocol[29]. Initially, BiOI nanoflake arrays (Figure S1) were electrodeposited on fluorine-doped tin dioxide (FTO). Subsequently, the $BiVO_4$ photoanode was obtained through further annealing with vanadyl acetylacetonate at elevated temperatures. The scanning electron microscopy (SEM) image in Figure 1a depicts the as-prepared $BiVO_4$ photoanode, showcasing a typical nanorod array structure with an average diameter of approximately 200 nm. Similarly, the transmission electron microscopy (TEM) image (Figure 1b) reveals irregular and adhesive nanoparticles (≈200 nm) constituting the morphology of the $BiVO_4$ photoanode. The high-resolution TEM (HRTEM) image (Figure 1c) demonstrates a lattice distance of 0.307 nm, consistent with the spacing of the (121) plane of monoclinic $BiVO_4$ (JCPDS#14-0688), confirming successful synthesis of $BiVO_4$[29]. The X-ray diffraction (XRD) pattern of the sample (Figure 1d) indicates the absence of characteristic peaks of vanadium oxides, with all diffraction peaks assignable to monoclinic $BiVO_4$ (JCPDS#14-0688), further confirming the crystal structure of $BiVO_4$ without any impurities. Additionally, the optical properties of the prepared $BiVO_4$ photoanode were examined via UV–vis diffuse reflectance spectrum (DRS), revealing an absorption edge at approximately 500 nm (Figure 1e), resulting in a bandgap of 2.54 eV according to the Tauc-plot (inset of Figure 1e)[30].

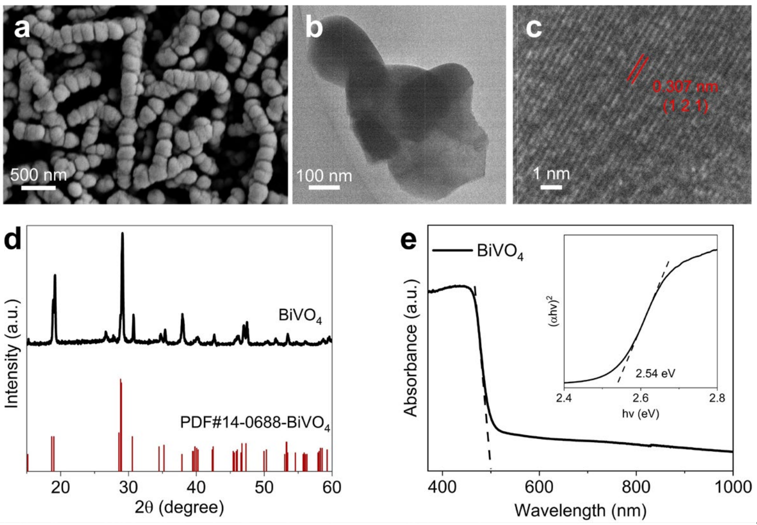

Figure 1. (a) SEM, (b) TEM, (c) HRTEM images and (d) the XRD pattern of the as-prepared $BiVO_4$. (e) The UV–vis DRS spectrum with the Tauc-plot of the $BiVO_4$ film.

2.2. Photoelectrochemical performance of the $BiVO_4$ photoanode

The PEC performance of the $BiVO_4$ photoanode was evaluated in electrolytes with various pH values (1, 7, 13) under one sun illumination (AM 1.5 G, 100 mW cm^{-2}). A three-electrode setup within

Preprints.org (www.preprints.org) | NOT PEER-REVIEWED | Posted: 17 May 2024 doi:10.20944/preprints202405.1127.v1

a quartz cell, employing Pt foil as the counter electrode and Ag/AgCl or Hg/HgO as the reference electrode, was utilized. Figure 2 illustrates the current density-potential profiles under dark and illumination conditions. In the absence of ethylene glycol in the reaction medium, the photocurrent density resulting from water oxidation via back illumination shows maximal variation. Notably, the highest photocurrent density occurs in pH=1 electrolyte (2.4 mA cm^{-2}), while values in pH=7 and 13 are 1.18 and 1.61 mA cm^{-2} at 1.23 V vs. RHE, respectively. The introduction of ethylene glycol leads to a significant increase in photocurrent density and a clear onset shift towards lower potentials, indicating easier oxidation of ethylene glycol than water[27,31]. Specifically, the photocurrent densities in pH=7 and 13 reach 3.44 and 3.12 mA cm^{-2}, respectively, while in pH=1, a highest photocurrent density of 7.10 mA cm^{-2} at 1.23 V vs. RHE was achieved. Apparently, the increase in pH decreases the photocurrent and increases onset potential, suggesting direct influence of proton on the catalytic oxidation reaction. Additionally, with increasing the applied potential, the photocurrent density in pH=13 experiences a decline, probably attributed to strongly alkaline-induced photocorrosion of $BiVO_4$[27].

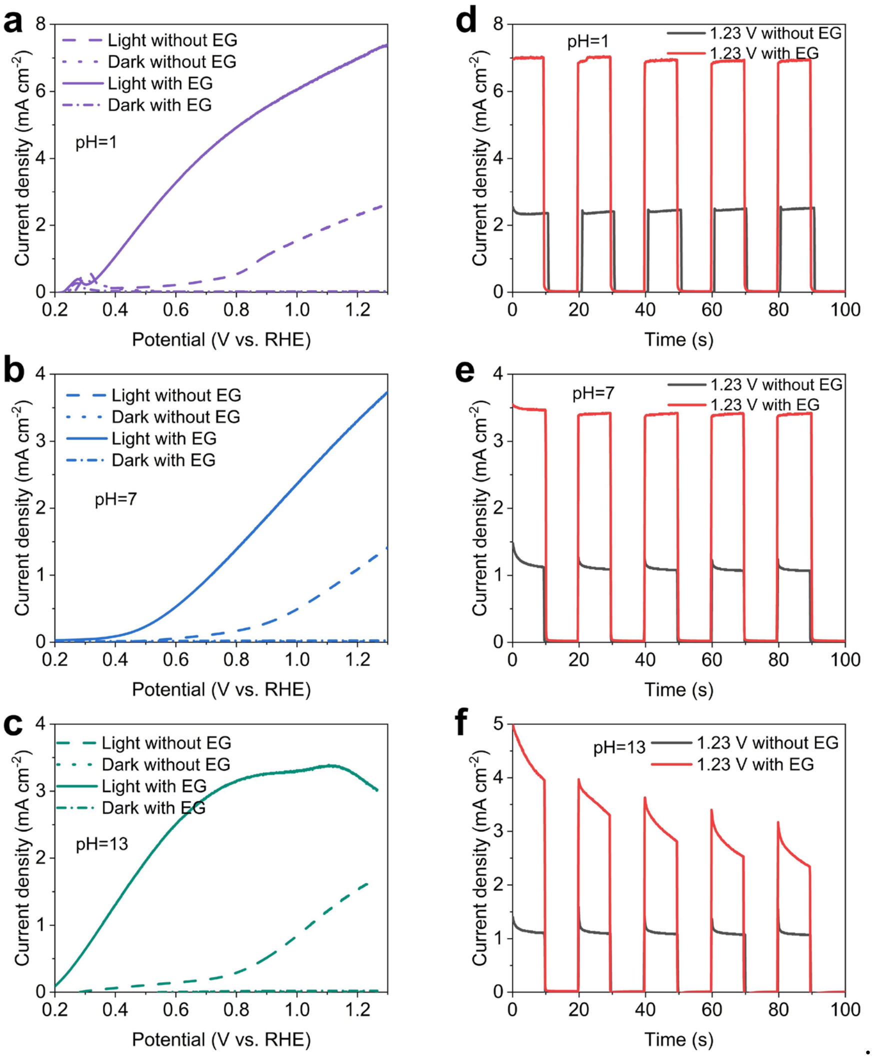

Figure 2. The PEC performance measured in various pH electrolytes with and without ethylene glycol. (a-c) Current density-potential profiles of the $BiVO_4$ photoanodes under dark and light illumination. (d-f) Chopped photocurrent density-time profiles of the $BiVO_4$ photoanodes at 1.23 V vs. RHE.

Figures 2d-f illustrate the chopped photocurrent profiles recorded at 1.23 V vs. RHE. In the absence of ethylene glycol, the slow kinetics of the water oxidation reaction result in the diffusion and accumulation of photogenerated holes at the $BiVO_4$ surface, leading to a transient spike at each

Preprints.org (www.preprints.org) | NOT PEER-REVIEWED | Posted: 17 May 2024 doi:10.20944/preprints202405.1127.v1

on-off cycle. Overall, the transient spike at pH=1 was weaker compared to pH=7 and 13, suggesting easier transfer of photo-generated holes for water oxidation reactions at pH=1, which therefore diminishes the chopped photocurrent spikes[31]. The addition of 0.5 M ethylene glycol not only significantly increases the photocurrent density but also reduces the photocurrent spike simultaneously. This observation indicates faster reaction kinetics for ethylene glycol oxidation than water oxidation. Moreover, an increase in reaction pH decreases the photocurrent density, possibly due to better ethylene glycol adsorption on $BiVO_4$ at lower pH, similar to previous reports, as will be demonstrated in subsequent experiments[27]. The enhanced ethylene glycol adsorption on $BiVO_4$ at lower pH facilitates the transfer of photogenerated holes for further oxidation reactions, thereby reducing the chopped photocurrent spikes. Additionally, the photocurrent density at pH=13 with ethylene glycol experiences a rapid decline within seconds, highlighting the high susceptibility of $BiVO_4$ to photocorrosion in alkaline environments.

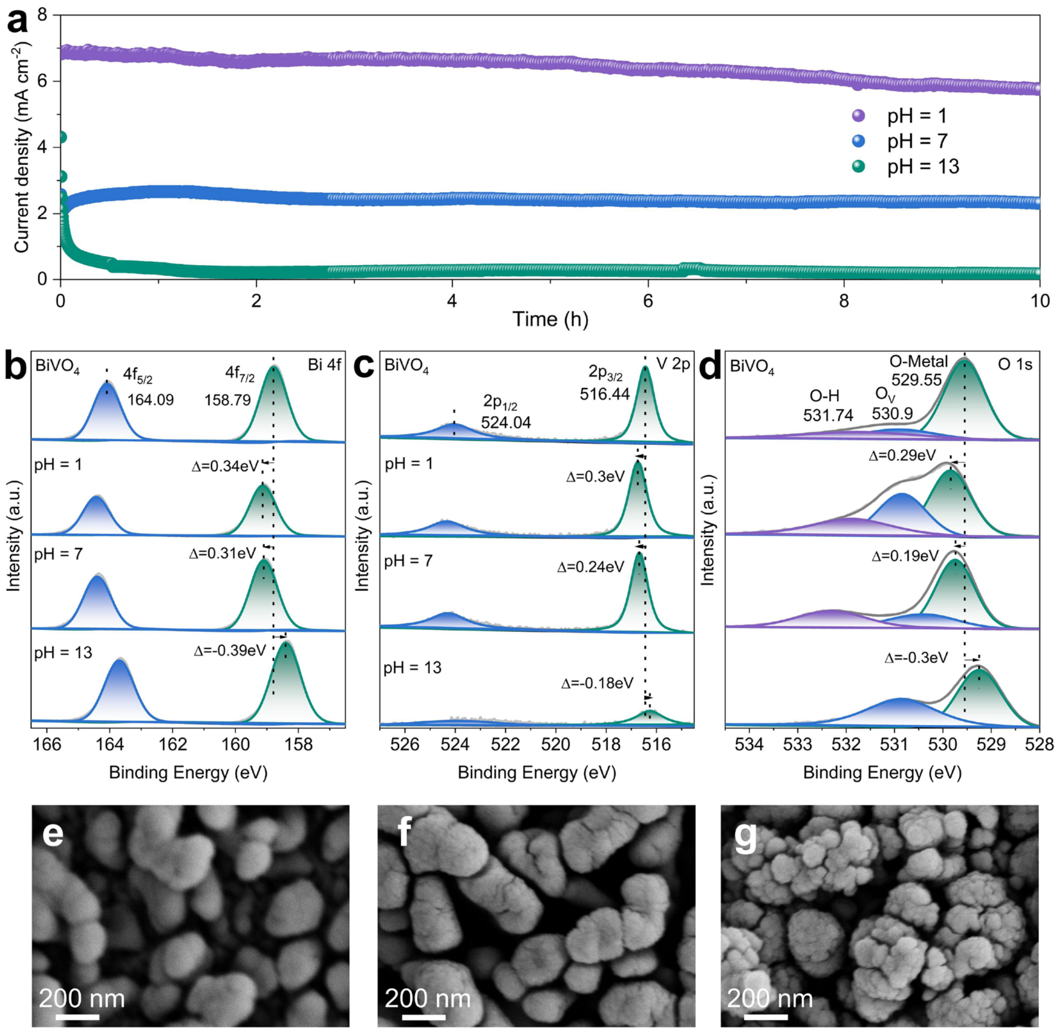

Figure 3. (a) Long time stability of $BiVO_4$ photoanode at 1.23 V vs. RHE in various pH with 0.5 M ethylene glycol under AM 1.5G, 100 mW cm^{-2} illumination. (b) Bi 4f, (c) V 2p and (d) O 1s XPS peaks of the $BiVO_4$ photoanode before and after the PEC tests in various pH electrolyte. SEM images of $BiVO_4$ photoanodes after the PEC tests in (e) pH=1, (f) pH=7 and (g) pH=13 with 0.5 M ethylene glycol.

The stability is also one of the most essential indicators for the practical application of a PEC system[32]. Therefore, the performance stability of PEC ethylene glycol oxidation was examined through current density-time curves at 1.23 V vs. RHE. As illustrated in Figure 3a, in the presence of ethylene glycol, the photocurrent density rapidly decreased for hundreds of seconds in pH=13. However, in pH=1 and 7, the photocurrent density maintained largely stability over an impressive

10-hour span. Additionally, the photocurrent of $BiVO_4$ in pH=1 with ethylene glycol was consistently significantly higher than in pH=7 and 13, suggesting that lower pH benefits the ethylene glycol oxidation activity[33]. The X-ray photoelectron spectroscopy (XPS) measurements were further carried out to study the changes in chemical states of the elements in the $BiVO_4$ photoanode before and after the PEC tests[34]. As presented in Figures 3b, c, the Bi 4f7/2, Bi 4f5/2, V 2p3/2, and V 2p1/2 XPS peaks of the $BiVO_4$ photoanode after the PEC test in pH=13 electrolyte shift to lower binding energy compared to pristine $BiVO_4$, indicating an increase in electron cloud density around Bi, V and O atoms probably due to the formation of oxygen vacancies[35–37], which led to the charge density of Bi and V are increased after the PEC test. More interestingly, the Bi 4f peaks (Figure 3b), V 2p (Figure 3c), and O 1s XPS peaks (Figure 3d) of $BiVO_4$ after testing in pH=1 and 7 moved to higher binding energy compared with pristine $BiVO_4$, suggesting the electron density reduction in the elements. These results imply the increase in oxidized states of $BiVO_4$ after ethylene glycol oxidation reaction[38,39]. Furthermore, the characteristic peaks of Bi element could be detected after the PEC stability tests, but their contents have been slightly decreased compared with the pristine samples, which can be assigned to the photo-induced Bi^{3+} dissolution from the $BiVO_4$ lattices[23]. Similarly, the peak intensity of V element has also been decreased, indicating a large amount of V element dissolution, leading to a significant decrease in stability in pH=13 electrolyte. SEM images were also obtained before and after the PEC tests (Figure 3e-g). The SEM images of the $BiVO_4$ photoanodes after the stability test in pH=1 and 7 demonstrate that the nanoporous structure was slightly destroyed compared to the initial $BiVO_4$ photoanode (Figure 1a). Surprisingly, the structure is completely destroyed after the PEC test in pH=13 electrolyte, which is consistent with the decay of the current density-time curve. In contrast, the XRD patterns were acquired after testing in pH=1 and 13 (Figure S2), which illustrate that the photoanodes maintain their structures. While the peak intensity was thoroughly weaken, which is consistent with the stability results.

2.3. Charge transport and dynamics in PEC ethylene glycol oxidation

To elucidate the influence of pH on the oxidation kinetics of the $BiVO_4$ photoanode, the overpotentials of the $BiVO_4$ photoanodes for ethylene glycol oxidation were recorded in dark with differing pH levels, as depicted in Figure 4a[33]. In the absence of ethylene glycol, the minimum overpotential was observed in the electrolyte with pH=7, signifying the optimal catalytic activity at this pH. In contrast, the most pronounced increase in current density for ethylene glycol oxidation in the electrolyte with pH=1 was noted in comparison to the pH=7 and 13 environments, suggesting the enhanced electrocatalytic activity due to the accelerated reaction kinetics under low pH conditions. Commonly, Na_2SO_3 was used as a hole scavenger to evaluate the charge injection efficiency on the surface of the photoanodes[29]. As demonstrated in Figure 4b, the addition of Na_2SO_3 significantly enhanced the PEC oxidation current density and, however, the current density for the ethylene glycol oxidation reaction consistently outperformed that of the sulfite oxidation in pH=1 and pH=13 electrolytes within the potential range of 0.68-1.25 and 0.32-1.26 V vs. RHE respectively, in which $BiVO_4$ exhibits faster ethylene glycol oxidation kinetics than that of Na_2SO_3[40]. This may suggest that the high current density was not only attributed to the photoelectric conversion of the $BiVO_4$ photoanode, but also to an additional current from the photo-driven ethylene glycol oxidation process[30].

Preprints.org (www.preprints.org) | NOT PEER-REVIEWED | Posted: 17 May 2024 doi:10.20944/preprints202405.1127.v1

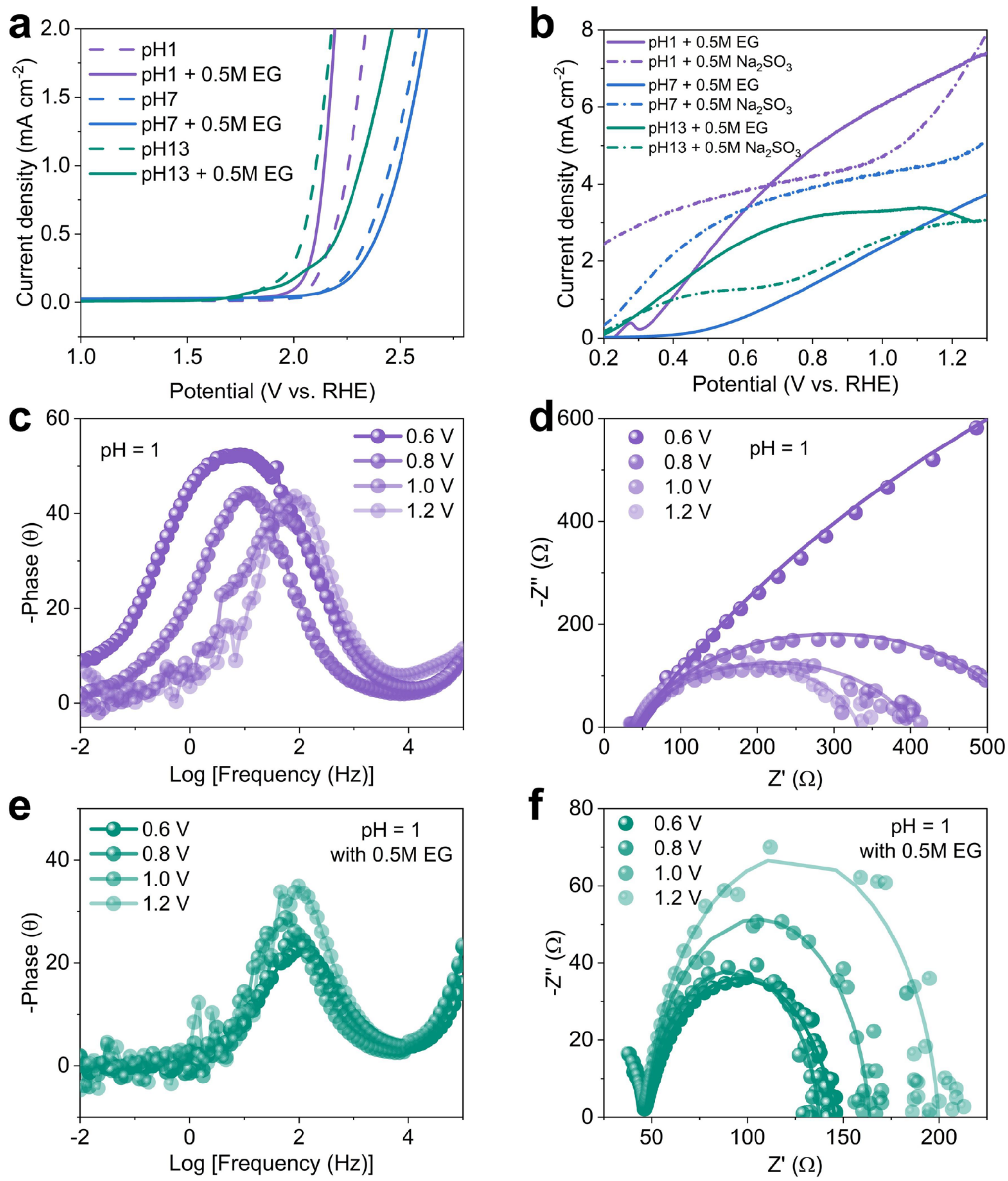

Figure 4. (a) LSV curves measured in dark. (b) LSV curves obtained in electrolytes with variable pH, with and without ethylene glycol and Na_2SO_3. Bode plots measured in different electrolytes at varying potentials (c) without and (e) with ethylene glycol. Nyquist plots recorded at distinct potentials in different electrolytes (d) without and (f) with ethylene glycol.

Electrochemical impedance spectroscopy (EIS) was employed to probe the charge and mass transfer processes under varying applied potentials in light[41]. The EIS spectra without ethylene glycol (Figure 4c, d) reveal a frequency peak decrease and shift towards higher frequencies and a decrease in the impedance semicircle diameter as bias increases, indicative of reduced faradaic resistance and an accelerated surface reaction rate. Upon the introduction of ethylene glycol (Figure 4e, f), the frequency peak remained nearly unchanged and the impedance semicircle expands with increasing bias, signifying that the intensified ethylene glycol oxidation process hampers the rapid desorption of reaction intermediates, thereby elevating the resistance, consistent with previous reports[27,42].

2.4. Product analysis and reaction mechanism of PEC ethylene glycol oxidation

The oxidation products of ethylene glycol over $BiVO_4$ at 1.23 V vs. RHE in various pH electrolytes containing 0.5 M ethylene glycol were analyzed under AM 1.5G illumination (100 mW

Preprints.org (www.preprints.org) | NOT PEER-REVIEWED | Posted: 17 May 2024 doi:10.20944/preprints202405.1127.v1

cm^{-2}) over a period of 10 hours[40,43]. The ^{1}H NMR spectra (Figure 5a) clearly shows the presence of formic acid, internal standard (maleic acid), H_2O, and ethylene glycol at 8.2, 6.0, 4.9, and 3.5 ppm, respectively[19,44]. Comparative analysis of the ^{1}H NMR spectra from electrolytes after 10 hours of stability testing at 1.23 V revealed selective oxidation of ethylene glycol to formic acid (Figure 5a, b). The highest yield of formic acid was achieved in the electrolytes with pH=1, suggesting that a strongly acidic environment favors the oxidation of ethylene glycol to formic acid.

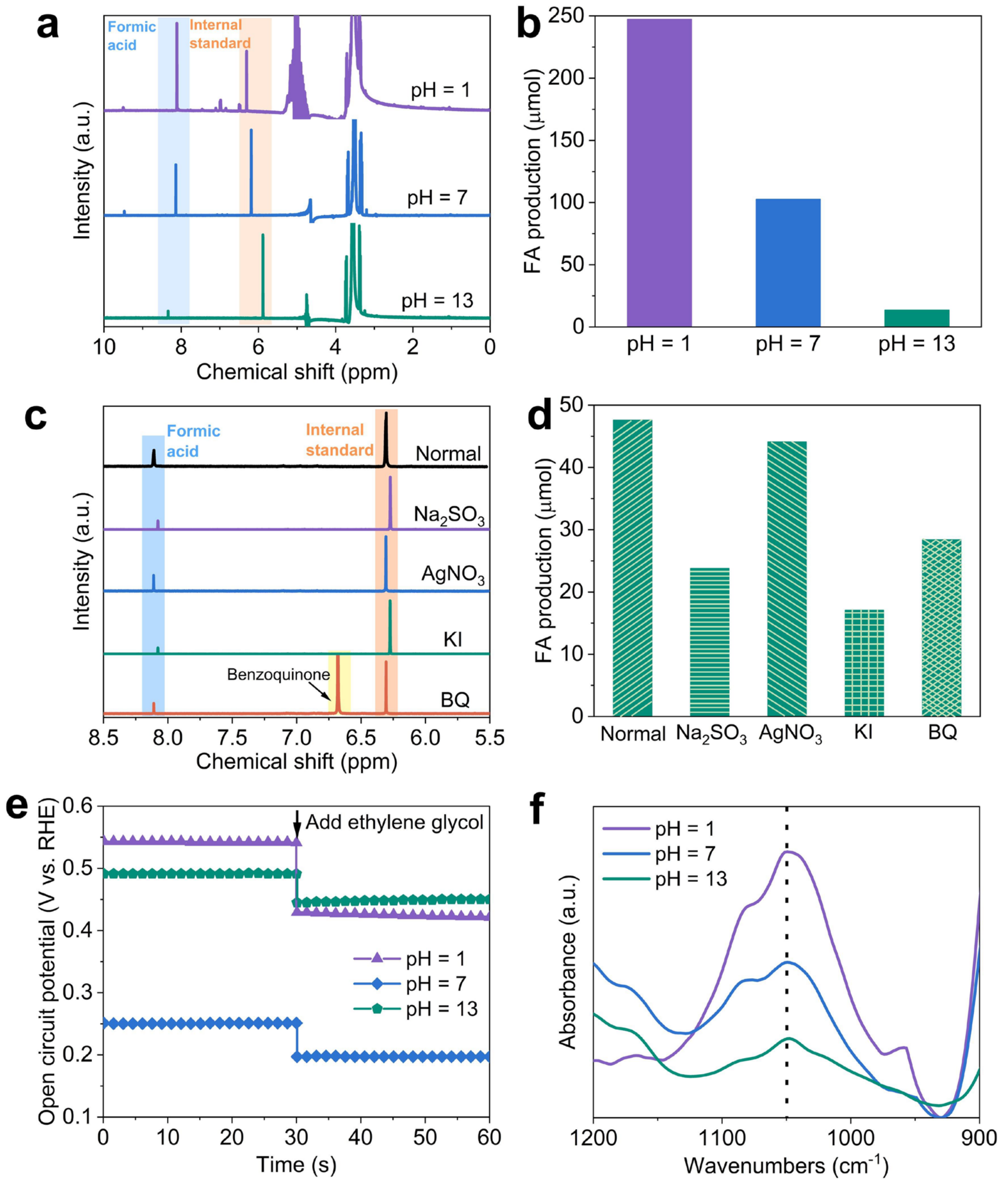

Figure 5. (a) ^{1}H NMR spectra (400 MHz, D_2O) of formic acid after 10-h ethylene glycol oxidation at 1.23 V vs. RHE on $BiVO_4$ in various electrolytes. (b) FA production in various electrolytes with ethylene glycol. (c) ^{1}H NMR spectra (400 MHz, D_2O) of formic acid after 2-h ethylene glycol oxidation at 1.23 V vs. RHE on $BiVO_4$ in the presence of various radical scavengers. (d) FA production in the presence of various radical scavengers (5 mM) for 2 hours (Normal, no scaven-ger; Na_2SO_3 as the hole scavenger, $AgNO_3$ as the electron scavenger, KI as the •OH radical scav-enger, BQ as the superoxide anion radicals). (e) Variation of open-circuit voltage in different pH conditions. (f) ATR-FTIR spectra of the $BiVO_4$ photoanodes after immersion in different electrolytes.

To understand the PEC oxidation mechanism, radical quenching experiments were conducted[45,46]. As depicted in Figure 5c-d, the use of Na_2SO_3 as a hole scavenger nearly halted formic acid (FA) production, underscoring the crucial role of photo-generated holes in the oxidation

Preprints.org (www.preprints.org) | NOT PEER-REVIEWED | Posted: 17 May 2024 doi:10.20944/preprints202405.1127.v1

of ethylene glycol. The addition of the electron scavenger $AgNO_3$ displayed minimal effect on FA yield. Additionally, when potassium iodide (KI) was employed to quench •OH radicals, there was a notable reduction in FA yield. In contrast, trapping superoxide anion radicals (•O_2^-) with benzoquinone (BQ) caused significant reduction of the FA production. These findings indicate that the photogenerated hole, •OH and superoxide anion radicals are involved in the PEC oxidation of ethylene glycol.

The adsorption of ethylene glycol species plays a critical role in the electrocatalytic oxidation process in the electrolyte. The open-circuit voltage, which is influenced by the adsorption species in the Helmholtz layer[47], reflects the adsorption behavior of ethylene glycol on $BiVO_4$ under different pH conditions. The open circuit potential (OCP) measurements (Figure 5e) demonstrate the effect of organic adsorbates on the inner Helmholtz layer[48]. Considering that the redox potential of ethylene glycol oxidation is lower than that of water, the contact between $BiVO_4$ and the electrolyte results in a reduced equilibrium potential through electron transfer with the ethylene glycol-containing electrolyte. The addition of ethylene glycol significantly lowers the OCP in pH=1 by 120 mV compared to pH=7 (Δ = 54 mV) and pH=13 (Δ = 41 mV), indicating more favorable adsorption of ethylene glycol on $BiVO_4$ at pH=1[49]. This trend suggests that increasing pH leads to higher OH^- concentrations, which in turn decreases ethylene glycol adsorption. Further confirmation of ethylene glycol adsorption behavior was obtained through attenuated total reflectance Fourier-transform infrared spectroscopy (ATR-FTIR) tests (Figure 5f). The results of ATR-FTIR spectroscopy revealed a new peak at 1050 cm^{-2}[50]corresponding to the stretching vibrational adsorption peak of the C–O bond on $BiVO_4$ after exposure to ethylene glycol solutions at varying pH levels. The highest peak intensity was observed after immersion in pH=1, indicating enhanced adsorption of ethylene glycol onto the $BiVO_4$ surface under acidic conditions. These results of the open-circuit voltage and ATR-FTIR measurements collectively confirm that the ethylene glycol adsorption on the $BiVO_4$ surface is most favorable at pH=1, thereby maximizing the activity of the ethylene glycol oxidation reaction at this pH level.

3. Materials and Methods

3.1. Chemicals and Materials

Bismuth nitrate pentahydrate ($Bi(NO_3)_3{\cdot}5H_2O$, analytical reagent grade), p-benzoquinone (≥98.0%), and vanadyl acetylacetonate ($VO(acac)_2$) were obtained from Sigma-Aldrich, Co. Ltd. (USA). Potassium iodide (KI, analytical reagent grade), dimethyl sulfoxide (DMSO, analytical reagent grade), glycerol ($C_3H_8O_3$, analytical reagent grade), ethylene glycol ($C_2H_6O_2$, analytical reagent grade), and nitric acid (HNO_3) were supplied by Sinopharm Chemical Reagent Co., Ltd. Fluorine-doped tin oxide (FTO, dimensions 10*30*2.2 mm, resistance 17 Ω) glass substrates were sourced from Luoyang Guluo Glass Technology Co., Ltd. All chemicals were of analytical grade and were used as received without any further purification.

3.2. Preparation of the $BiVO_4$ Photoanode

The $BiVO_4$ thin films were prepared using a modified method previously described by Choi[29], which involves electrodeposition followed by air annealing. Initially, 0.97 g of $Bi(NO_3)_3{\cdot}5H_2O$ was dissolved in 50 mL of 0.4 M KI solution, and the pH was adjusted to 1.7 using HNO_3 to prepare solution A. Subsequently, 0.4972 g of p-benzoquinone (0.23 M) was dissolved in 20 mL of anhydrous ethanol to form solution B. The solution B was then gradually added to the solution A under vigorous stirring for 30 minutes at room temperature, resulting in the solution C. The BiOI films were fabricated through electrodeposition using a three-electrode system, with the FTO glass serving as the working electrode, a Pt plate as the counter electrode, and an Ag/AgCl electrode as the reference electrode. The solution C was used as the electrolyte. Electrodeposition was carried out at a constant potential of −0.1 V vs. Ag/AgCl for 540 seconds. The obtained orange BiOI precursors were washed with deionized water, dried with N_2, and subsequently coated with a DMSO solution con-taining 0.2 M $VO(acac)_2$, referred to as the solution D. To finalize the $BiVO_4$ pho-toanodes, 0.11 mL of the solution

Preprints.org (www.preprints.org) | NOT PEER-REVIEWED | Posted: 17 May 2024 doi:10.20944/preprints202405.1127.v1

D was applied to each BiOI electrode (1 × 2 cm^2). The assemblies were then heated in air at a rate of 2 °C/min to 450 °C and held at this temperature for 120 minutes. After natural cooling, the obtained samples were immersed in 1 M NaOH solution for 30 minutes with gentle stirring to eliminate any residual vanadium oxide. The final $BiVO_4$ film electrodes were thus obtained.

3.3. Characterization

The crystalline structures of the samples were analyzed using X-ray diffraction (XRD, Bruker D2 Phaser) and Raman spectroscopy (HORIBA XploRA Nano). The mor-phology and structural details were investigated via field emission scanning electron microscopy (SEM, HITACHI S-4800) and transmission electron microscopy (TEM, JEOL JEM-2100F). The optical properties were assessed through UV-Vis-IR spectrophotometry (UV-2600) equipped with an integrating sphere. Surface compositions and electronic states were studied using X-ray photoelectron spectroscopy (XPS, X Per3 Powder). Proton nuclear magnetic resonance (^1H NMR) spectra were recorded on a Bruker Advance III HD400 spectrometer.

3.4. Photoelectrochemical Measurements

The PEC experiments were conducted using a CHI660E electrochemical workstation (Shanghai Chen Hua Instruments Co., China) in a three-electrode configuration. The working electrode was the as-prepared $BiVO_4$ photoanode with an area of 1 × 1 cm^2, illuminated from behind. The reference and counter electrodes were an Ag/AgCl electrode and a 1 × 1 cm^2 Pt sheet, respectively. The electrolytes used were: (1) 0.1 M HNO_3 acidic solution, with or without ethylene glycol, at pH=1; (2) a neutral solution adjusted to pH=7 using 1 M NaOH and 0.1 M HNO_3; and (3) a 0.1 M NaOH alkaline solution at pH=13. The light source was a 300W xenon lamp (PLS-SXE300D) equipped with an AM 1.5G filter, set to an intensity of 100 mW cm^{-2}. Linear sweep voltammetry (LSV) curves were recorded from 0.2 to 1.3 V vs. RHE at a scan rate of 10 mV/s, both with and without 0.5 M ethylene glycol. The impedance spectra were obtained from 0.01 to 10^5 Hz with a 5mV amplitude under AM 1.5G illumination, at potentials ranging from 0.6 V to 1.2 V vs. RHE. The stability test for the $BiVO_4$ photoanodes in the presence of ethylene glycol was conducted across various pH electrolytes with 0.5 M ethylene glycol at 1.23 V vs. RHE under AM 1.5G illumination for 10 hours. The applied potentials vs. Ag/AgCl, Hg/HgO were converted to the RHE scale using the Nernst equation:

$$E_{RHE} = E_{Ag/AgCl} + 0.059\ pH + 0.1972$$

$$E_{RHE} = E_{Hg/HgO} + 0.059\ pH + 0.098$$

3.5. The product analysis

To quantitatively assess the products, ^1H NMR data were acquired using an Advance III HD400 spectrometer (400 MHz). Initially, the electrolyte after the stability test at an applied voltage of 1.23 V vs. RHE for 10 hours for ethylene glycol oxidation under AM 1.5G light at 100 mW cm^{-2} was collected. Then, 500 μL of this electrolyte was transferred to an NMR tube, to which 40 μL of a 20 mM maleic acid solution and 100 μL of deuterium water (D_2O) were added. The mixture was sonicated briefly to ensure homogeneity. The resultant ^1H NMR spectrum revealed peaks for ethylene glycol, maleic acid, and D_2O at 3.5, 5.9, and 4.8 ppm, respectively. All NMR data were analyzed using MestReNova software.

4. Conclusions

In summary, our research underscores the profound influence of electrolyte pH on the PEC oxidation of ethylene glycol using $BiVO_4$, optimizing photocurrent output. At a pH=1 electrolyte, we observed an enhancement in charge injection efficiency, leading to a superior photocurrent density of 7.1 mA cm^{-2} at 1.23 V vs. RHE and the highest yield of formic acid, compared to neutral and alkaline conditions (pH=7 and pH=13). The comprehensive experimental analysis confirms that the superior adsorption properties of $BiVO_4$ on ethylene glycol under acidic conditions are a key factor in the increased oxidation reaction activity. The mechanistic investigation of the PEC process indicates the

 doi:10.20944/preprints202405.1127.v1

involvement of multiple reaction pathways in the oxidation of ethylene glycol. This study not only highlights the critical impact of pH in modulating PEC biomass oxidation but also accentuates the promising potential of the PEC approach in the sustainable synthesis of valuable chemicals and energy carriers.

Supplementary Materials: The following supporting information can be downloaded at the website of this paper posted on Preprints.org. Figure S1: A Top-view SEM image of the BiOI nanoflake array; Figure S2: XRD patterns of the $BiVO_4$ photoanodes after testing in various electrolytes in the presence of ethylene glycol.

Author Contributions: Conceptualization, J-J.W. and J-Y.C.; methodology, T-T.L. and L.C.; software, L.C.; formal analysis, T-T.L.; investigation, J-Y.C. and T-T.L.; data curation, J-Y.C. and L.C.; writing—original draft preparation, J-Y.C.; writing—review and editing, J-J.W.; supervision, J-J.W.; funding acquisition, J-J.W. All authors have read and agreed to the published version of the manuscript.

Funding: This research was funded by the National Natural Science Foundation of China, grant number Nos. 22279075; the Shandong Provincial Natural Science Foundation, grant number No. ZR2020YQ09.

Institutional Review Board Statement: Not applicable.

Informed Consent Statement: Not applicable.

Data Availability Statement: Data will be made available on request.

Conflicts of Interest: The authors declare no conflicts of interest.

References

1. Lu, H.; Diaz, D.J.; Czarnecki, N.J.; Zhu, C.; Kim, W.; Shroff, R.; Acosta, D.J.; Alexander, B.R.; Cole, H.O.; Zhang, Y.; Lynd, N.A.; Ellington, A.D.; Alper, H.S., Machine learning-aided engineering of hydrolases for PET depolymerization. *Nature* **2022**, *604*, 662-667.
2. Tang, T.; Liu, X.; Luo, X.; Xue, Z.; Pan, H.-R.; Fu, J.; Yao, Z.-C.; Jiang, Z.; Lyu, Z.-H.; Zheng, L.; Su, D.; Zhang, J.-N.; Zhang, L.; Hu, J.-S., Unconventional Bilateral Compressive Strained Ni–Ir Interface Synergistically Accelerates Alkaline Hydrogen Oxidation. *J. Am. Chem. Soc.* **2023**, *145*, 13805-13815.
3. Yin, Z.-H.; Huang, Y.; Song, K.; Li, T.-T.; Cui, J.-Y.; Meng, C.; Zhang, H.; Wang, J.-J., Ir Single Atoms Boost Metal–Oxygen Covalency on Selenide-Derived NiOOH for Direct Intramolecular Oxygen Coupling. *J. Am. Chem. Soc.* **2024**, *146*, 6846-6855.
4. Roger, I.; Shipman, M.A.; Symes, M.D., Earth-abundant catalysts for electrochemical and photoelectrochemical water splitting. *Nat. Rev. Chem.* **2017**, *1*, 0003.
5. Lu, T.; Li, T.; Shi, D.; Sun, J.; Pang, H.; Xu, L.; Yang, J.; Tang, Y., In situ establishment of Co/MoS_2 heterostructures onto inverse opal-structured N,S-doped carbon hollow nanospheres: Interfacial and architectural dual engineering for efficient hydrogen evolution reaction. *SmartMat* **2021**, *2*, 591-602.
6. Lewis, N.S., Research opportunities to advance solar energy utilization. *Science* **2016**, *351*, aad1920.
7. Ye, S.; Shi, W.; Liu, Y.; Li, D.; Yin, H.; Chi, H.; Luo, Y.; Ta, N.; Fan, F.; Wang, X.; Li, C., Unassisted Photoelectrochemical Cell with Multimediator Modulation for Solar Water Splitting Exceeding 4% Solar-to-Hydrogen Efficiency. *J. Am. Chem. Soc.* **2021**, *143*, 12499-12508.
8. Li, T.-T.; Cui, J.-Y.; Xu, M.; Song, K.; Yin, Z.-H.; Meng, C.; Liu, H.; Wang, J.-J., Efficient Acidic Photoelectrochemical Water Splitting Enabled by Ru Single Atoms Anchored on Hematite Photoanodes. *Nano Lett.* **2024**, *24*, 958-965.
9. Wu, S.; Zhu, Y.; Yang, G.; Zhou, H.; Li, R.; Chen, S.; Li, H.; Li, L.; Fontaine, O.; Deng, J., Take full advantage of hazardous electrochemical chlorine erosion to ultrafast produce superior NiFe oxygen evolution reaction electrode. *Chem. Eng. J.* **2022**, *446*, 136833.
10. Wang, X.; Xing, C.; Liang, Z.; Guardia, P.; Han, X.; Zuo, Y.; Llorca, J.; Arbiol, J.; Li, J.; Cabot, A., Activating the lattice oxygen oxidation mechanism in amorphous molybdenum cobalt oxide nanosheets for water oxidation. *J. Mater. Chem. A* **2022**, *10*, 3659-3666.
11. Wang, X.; Han, X.; Du, R.; Xing, C.; Qi, X.; Liang, Z.; Guardia, P.; Arbiol, J.; Cabot, A.; Li, J., Cobalt Molybdenum Nitride-Based Nanosheets for Seawater Splitting. *ACS Appl. Mater. Interfaces* **2022**, *14*, 41924-41933.
12. Yang, G.; Jiao, Y.; Yan, H.; Xie, Y.; Wu, A.; Dong, X.; Guo, D.; Tian, C.; Fu, H., Interfacial Engineering of MoO_2-FeP Heterojunction for Highly Efficient Hydrogen Evolution Coupled with Biomass Electrooxidation. *Adv. Mater.* **2020**, *32*, 2000455.
13. Korley, L.T.J.; III, T.H.E.; Helms, B.A.; Ryan, A.J., Toward polymer upcycling—adding value and tackling circularity. *Science* **2021**, *373*, 66-69.

 doi:10.20944/preprints202405.1127.v1

14. Ellis, L.D.; Rorrer, N.A.; Sullivan, K.P.; Otto, M.; McGeehan, J.E.; Román-Leshkov, Y.; Wierckx, N.; Beckham, G.T., Chemical and biological catalysis for plastics recycling and upcycling. *Nat. Catal.* **2021**, *4*, 539-556.
15. Kalathil, S.; Miller, M.; reisner, E., Microbial Fermentationof Polyethylene Terephthalate (PET) Plastic Waste for the Productionof Chemicals or Electricity**. *Angew. Chem. Int. Ed.* **2022**, *61*, e202211057.
16. Zhang, X.; Wei, R.; Yan, M.; Wang, X.; Wei, X.; Wang, Y.; Wang, L.; Zhang, J.; Yin, S., One-Pot Synthesis Inorganic – Organic Hybrid PdNi Bimetallenes for PET Electrocatalytic Value-Added Transformation. *Advanced Functional Materials* **2024**, 2401796.
17. Pang, J.; Zheng, M.; Sun, R.; Wang, A.; Wang, X.; Zhang, T., Synthesis of ethylene glycol and terephthalic acid from biomass for producing PET. *Green Chem.* **2016**, *18*, 342-359.
18. Bianchini, C.; Shen, P.K., Palladium-Based Electrocatalysts for Alcohol Oxidation in Half Cells and in Direct Alcohol Fuel Cells. *Chem. Rev.* **2009**, *109*, 4183-4206.
19. Li, J.; Li, L.; Ma, X.; Han, X.; Xing, C.; Qi, X.; He, R.; Arbiol, J.; Pan, H.; Zhao, J.; Deng, J.; Zhang, Y.; Yang, Y.; Cabot, A., Selective Ethylene Glycol Oxidation to Formate on Nickel Selenide with Simultaneous Evolution of Hydrogen. *Adv. Sci.* **2023**, *10*, 2300841.
20. Liu, W.-J.; Xu, Z.; Zhao, D.; Pan, X.-Q.; Li, H.-C.; Hu, X.; Fan, Z.-Y.; Wang, W.-K.; Zhao, G.-H.; Jin, S.; Huber, G.W.; Yu, H.-Q., Efficient electrochemical production of glucaric acid and H_2 via glucose electrolysis. *Nat. Commun.* **2020**, *11*, 265.
21. Zhang, Q.; Wang, Y.; Zhang, W.; Yao, X.; Liang, Q., Hydrogel Enabled Dual-Shielding Improves Efficiency and Stability of $BiVO_4$ Based Photoanode for Solar Water Splitting. *Advanced Functional Materials* **2024**, 2314973.
22. Liu, B.; Wang, X.; Zhang, Y.; Xu, L.; Wang, T.; Xiao, X.; Wang, S.; Wang, L.; Huang, W., A $BiVO_4$ Photoanode with a VO_x Layer Bearing Oxygen Vacancies Offers Improved Charge Transfer and Oxygen Evolution Kinetics in Photoelectrochemical Water Splitting. *Angew. Chem. Int. Ed.* **2023**, *62*, e202217346
23. Zhang, B.; Yu, S.; Dai, Y.; Huang, X.; Chou, L.; Lu, G.; Dong, G.; Bi, Y., Nitrogen-incorporation activates $NiFeO_x$ catalysts for efficiently boosting oxygen evolution activity and stability of $BiVO_4$ photoanodes. *Nat. Commun.* **2021**, *12*, 6969-6976.
24. Han, Y.; Chang, M.; Zhao, Z.; Niu, F.; Zhang, Z.; Sun, Z.; Zhang, L.; Hu, K., Selective Valorization of Glycerol to Formic Acid on a $BiVO_4$ Photoanode through NiFe Phenolic Networks. *ACS Appl. Mater. Interfaces* **2023**, *15*, 11678-11690.
25. Lin, C.; Dong, C.; Kim, S.; Lu, Y.; Wang, Y.; Yu, Z.; Gu, Y.; Gu, Z.; Lee, D.K.; Zhang, K.; Park, J.H., Photo-Electrochemical Glycerol Conversion over a Mie Scattering Effect Enhanced Porous $BiVO_4$ Photoanode. *Adv. Mater.* **2023**, *35*, 2209955.
26. Vo, T.-G.; Kao, C.-C.; Kuo, J.-L.; Chiu, C.-c.; Chiang, C.-Y., Unveiling the crystallographic facet dependence of the photoelectrochemical glycerol oxidation on bismuth vanadate. *Applied Catalysis B: Environmental* **2020**, *278*, 119303.
27. Liu, D.; Liu, J.-C.; Cai, W.; Ma, J.; Yang, H.B.; Xiao, H.; Li, J.; Xiong, Y.; Huang, Y.; Liu, B., Selective photoelectrochemical oxidation of glycerol to high value-added dihydroxyacetone. *Nat. Commun.* **2019**, *10*, 1779-1787.
28. Nascimento, L.L.; Marinho, J.Z.; dos Santos, A.L.R.; de Faria, A.M.; Souza, R.A.C.; Wang, C.; Patrocinio, A.O.T., Photoelectrochemical reforming of glycerol by Bi_2WO_6 photoanodes: Role of the electrolyte pH on the H_2 evolution efficiency and product selectivity. *Appl. Catal. A., Gen.* **2022**, *646*, 118867.
29. Kim, T.W.; Choi, K.-S., Nanoporous $BiVO_4$ Photoanodes with Dual-Layer Oxygen Evolution Catalysts for Solar Water Splitting. *Science* **2014**, *343*, 990-994.
30. Wang, Z.Q.; Guo, Y.H.; Liu, M.; Liu, X.L.; Zhang, H.P.; Jiang, W.Y.; Wang, P.; Zheng, Z.K.; Liu, Y.N.; Cheng, H.F.; Dai, Y.; Wang, Z.Y.; Huang, B.B., Boosting H_2 Production from a $BiVO_4$ Photoelectrochemical Biomass Fuel Cell by the Construction of a Bridge for Charge and Energy Transfer. *Adv. Mater.* **2022**, *34*, 2201594.
31. Dotan, H.; Sivula, K.; Grätzel, M.; Rothschild, A.; Warren, S.C., Probing the photoelectrochemical properties of hematite (α-Fe_2O_3) electrodes using hydrogen peroxide as a hole scavenger. *Energy Environ. Sci.* **2011**, *4*, 958-964.
32. Lee, D.K.; Choi, K.-S., Enhancing long-term photostability of $BiVO_4$ photoanodes for solar water splitting by tuning electrolyte composition. *Nat. Energy.* **2018**, *3*, 53-60.
33. Jiang, T.; Wang, W.; Bi, Y.; Liang, Y.; Fu, J.; Wang, L.; Zhou, Q., Accelerating Surface Reaction Kinetics and Enhancing Bulk as well as Surface Charge Carrier Dynamics in Al/ Al_2O_3-Coated $BiVO_4$ Photoanode. *Advanced Functional Materials* **2024**, 2403396.
34. Chen, Y.; Li, X.; Yang, H.; Huang, Y., Systematic Constructing FeOCl/$BiVO_4$ Hetero-Interfacial Hybrid Photoanodes for Efficient Photoelectrochemical Water Splitting. *Small* **2024**, 2402406.
35. Li, X.; Wu, J.; Dong, C.; Kou, Y.; Hu, C.; Zang, J.; Zhu, J.; Ma, B.; Li, Y.; Ding, Y., Boosting photoelectrocatalytic oxygen evolution activity of $BiVO_4$ photoanodes via caffeic acid bridged to NiFeOOH. *Applied Catalysis B: Environment and Energy* **2024**, *353*.

 doi:10.20944/preprints202405.1127.v1

36. Pan, J.B.; Wang, B.H.; Wang, J.B.; Ding, H.Z.; Zhou, W.; Liu, X.; Zhang, J.R.; Shen, S.; Guo, J.K.; Chen, L.; Au, C.T.; Jiang, L.L.; Yin, S.F., Activity and Stability Boosting of an Oxygen-Vacancy-Rich $BiVO_4$ Photoanode by NiFe-MOFs Thin Layer for Water Oxidation. *Angew. Chem. Int. Ed.* **2020**, *60*, 1433-1440.
37. Wang, S.; Chen, P.; Yun, J.H.; Hu, Y.; Wang, L., An Electrochemically Treated $BiVO_4$ Photoanode for Efficient Photoelectrochemical Water Splitting. *Angew. Chem. Int. Ed.* **2017**, *56*, 8500-8504.
38. Choi, S.; Lee, S.A.; Yang, J.W.; Sohn, W.; Kim, J.; Cheon, W.S.; Park, J.; Cho, J.H.; Lee, C.W.; Jun, S.E.; Park, S.H.; Moon, J.; Kim, S.Y.; Jang, H.W., Boosted charge transport through Au-modified NiFe layered double hydroxide on silicon for efficient photoelectrochemical water oxidation. *J. Mater. Chem. A* **2023**, *11*, 17503-17513.
39. Lee, S.A.; Lee, T.H.; Kim, C.; Choi, M.-J.; Park, H.; Choi, S.; Lee, J.; Oh, J.; Kim, S.Y.; Jang, H.W., Amorphous Cobalt Oxide Nanowalls as Catalyst and Protection Layers on n-Type Silicon for Efficient Photoelectrochemical Water Oxidation. *ACS Catal.* **2019**, *10*, 420-429.
40. Wu, Y.-H.; Kuznetsov, D.A.; Pflug, N.C.; Fedorov, A.; Mueller, C.R., Solar-driven valorisation of glycerol on $BiVO_4$ photoanodes: effect of co-catalyst and reaction media on reaction selectivity. *J. Mater. Chem. A* **2021**, *9*, 6252-6260.
41. Klahr, B.; Gimenez, S.; Zandi, O.; Fabregat-Santiago, F.; Hamann, T., Competitive Photoelectrochemical Methanol and Water Oxidation with Hematite Electrodes. *ACS Appl. Mater. Interfaces* **2015**, *7*, 7653-7660.
42. Heo, N.; Jun, Y.; Park, J.H., Dye molecules in electrolytes: new approach for suppression of dye-desorption in dye-sensitized solar cells. *Sci. Rep.* **2013**, *3*, 1712-1717.
43. Wang, X.; Wei, X.; Zhang, R.; Yan, M.; Wei, R.; Zhang, X.; Zhu, Z.; Wang, Y.; Zhao, X.; Yin, S., Defect-rich Pd@PdOs nanobelts for electrocatalytic oxidation of ethylene glycol. *Inorg. Chem. Front.* **2024**, *11*, 2562-2569.
44. Deng, K.; Lian, Z.; Wang, W.; Yu, J.; Yu, H.; Wang, Z.; Xu, Y.; Wang, L.; Wang, H., Lattice Strain and Charge Redistribution of Pt Cluster/Ir Metallene Heterostructure for Ethylene Glycol to Glycolic Acid Conversion Coupled with Hydrogen Production. *Small* **2023**, *20*, 2305000.
45. Lin, C.; Shan, Z.; Dong, C.; Lu, Y.; Meng, W.; Zhang, G.; Cai, B.; Su, G.; Park, J.H.; Zhang, K., Covalent organic frameworks bearing Ni active sites for free radical-mediated photoelectrochemical organic transformations. *Sci. Adv.* **2023**, *9*, eadi9442.
46. Luo, L.; Chen, W.; Xu, S.-M.; Yang, J.; Li, M.; Zhou, H.; Xu, M.; Shao, M.; Kong, X.; Li, Z.; Duan, H., Selective Photoelectrocatalytic Glycerol Oxidation to Dihydroxyacetone via Enhanced Middle Hydroxyl Adsorption over a Bi_2O_3-Incorporated Catalyst. *J. Am. Chem. Soc.* **2022**, *144*, 7720-7730.
47. Yang, Y.; Xu, D.; Zhang, B.; Xue, Z.; Mu, T., Substrate molecule adsorption energy: An activity descriptor for electrochemical oxidation of 5-Hydroxymethylfurfural (HMF). *Chem. Eng. J.* **2022**, *433*, 133842.
48. Zhou, P.; Lv, X.; Tao, S.; Wu, J.; Wang, H.; Wei, X.; Wang, T.; Zhou, B.; Lu, Y.; Frauenheim, T.; Fu, X.; Wang, S.; Zou, Y., Heterogeneous-Interface-Enhanced Adsorption of Organic and Hydroxyl for Biomass Electrooxidation. *Adv. Mater.* **2022**, *34*, 2204089.
49. Shi, K.; Si, D.; Teng, X.; Chen, L.; Shi, J., Pd/$NiMoO_4$/NF electrocatalysts for the efficient and ultra-stable synthesis and electrolyte-assisted extraction of glycolate. *Nat. Commun.* **2024**, *15*, 2899.
50. Schnaidt, J.; Heinen, M.; Denot, D.; Jusys, Z.; Jürgen Behm, R., Electrooxidation of glycerol studied by combined *in situ* IR spectroscopy and online mass spectrometry under continuous flow conditions. *J. Electroanal. Chem* **2011**, *661*, 250-264.